Dielectric relaxation phenomena in $Cd_2Nb_2O_7$ ferroelectric-ferroelastics

1994 J. Phys.: Condens. Matter 6 2787

(http://iopscience.iop.org/0953-8984/6/14/016)

J. Phys.: Condens. Matter 6 (1994) 2787–2798. Printed in the UK

Dielectric relaxation phenomena in $Cd_2Nb_2O_7$ ferroelectric–ferroelastics

N N Kolpakova†, R Margraf‡ and M Polomska‡

† Ioffe Physico-Technical Institute, RAS, Polytechnicheskaya 26, 194021 St Petersburg, Russia

‡ Institute of Molecular Physics, PAS, Smoluchowskiego 17/19, 60179 Poznań, Poland

Received 30 April 1993, in final form 18 October 1993

Abstract. Low-frequency (1 kHz–1 MHz) dielectric permittivity studies of $Cd_2Nb_2O_7$ single crystals under a uniaxial pressure of 0 MPa $\leqslant X \lesssim 4$ MPa in a wide measurement AC field strength range of 1 V cm^{-1} $< \mathcal{E} <$ 110 V cm^{-1} are reported. An analysis of the experimental data reveals that we are concerned with two Debye-type relaxation mechanisms in the ferroelectric phase: $T < T_c$ (= 196 K) $< T_s$ (= 205 K). Both of these are manifested when the frequency or the field $\mathcal{E}$ is changed, while only the domain relaxation is manifested with increasing pressure. The relaxation caused by domain wall motion and by reorientation of spontaneous polarization of domains dominates. The second relaxation has its origin in the orientational polarizability of the steady Cd^{2+}–O^{2-} (seventh) dipoles in the measurement AC field. The disordered Cd^{2+}–O^{2-} dipole system in the pyrochlore network is formed in the paraelectric phase. Their orientational polarizability in the external electric field results in an anomalously high static dielectric permittivity $\varepsilon_0 = 450$ compared with $\varepsilon_\infty = 5.43$ at room temperature, as well as dielectric dispersion above T_c and T_s.

1. Introduction

In general, the oxides $A_2B_2O_7$ can be divided into several types according to the crystal structure: pyrochlores ($Cd_2Ta_2O_7$, $Pb_2Ta_2O_7$, etc), slab perovskites ($Sr_2Nb_2O_7$) and weberites ($Sr_2Sb_2O_7$, $Ca_2Sb_2O_7$, etc) [1–3]. Cadmium pyroniobate ($Cd_2Nb_2O_7$) belongs to the cubic oxide pyrochlores of $A_2^{2+}B_2^{5+}O_6Z$ type (Z denotes the 'seventh' oxygen ion O^{2-}, S^{2-}, OH^- or F^-). Its structure at room temperature (paraelectric phase) is described by the cubic space group O_h^7 ($Fd3m$) [3]. For comparison, the diamond structure is also described by the space group O_h^7 ($Fd3m$) [4]. The very high symmetry of the paraelectric phase of $Cd_2Nb_2O_7$ makes a large variety of phase transitions possible and makes invoking the high-symmetric hypothetical parent phase for analysis of the sequence of phase transitions unnecessary [5]. Below $T_s = 205$ K, $Cd_2Nb_2O_7$ is ferroelastic [6], below $T_c = 196$ K it is ferroelectric too [3, 6] and it remains both ferroelectric and ferroelastic down to 4 K [7, 8]. With ferroelastic and ferroelectric domains as a background, there appears an intermediate phase within the temperature range of 46–85 K [7, 9] and a glassy state below 18 K [10, 11]. In fact, the behaviour of $Cd_2Nb_2O_7$ is rather complicated and there are no analogues to it as far as ferroelectrics are concerned [1].

Within the temperature range 100–300K, which includes the ferroelastic and ferroelectric transition temperatures, the electric properties of $Cd_2Nb_2O_7$ at low frequencies (1 kHz–1 MHz) are atypical of ferroelectrics. At room temperature, the static dielectric permittivity $\varepsilon_0 = 450$ is unusually high compared with $\varepsilon_\infty = n^2 = 5.43$ [3, 6, 12]. Dielectric dispersion

0953-8984/94/142787+12$19.50

takes place not only in the ferroelectric phase but also in the paraelectric phase [12]. In the ferroelectric phase, there is a peak in $\varepsilon'(T)$ at $T_{max} < T_c < T_s$ along the $[111]_{cub}$, $[100]_{cub}$ and $[110]_{cub}$ axes which occurs below 1 MHz and its magnitude is frequency dependent [3, 12–15]. The origin of the peak is questionable. This peak cannot be assigned to the existence of a phase transition because at T_{max} no changes in domain structure [6, 7], refractive index [13], specific heat or spontaneous polarization [16] are observed. The peak may originate from the relaxation processes which take place in the ferroelectric phase of $Cd_2Nb_2O_7$ [6, 12–16]. However, here we face another problem, namely the mechanisms responsible for the dielectric relaxation phenomena in the ferroelectric phase of this pyrochlore are not clarified. The only fact known is that there is more than one mechanism [12, 17]. The major relaxation is caused by the motion of domain walls which are very mobile in $Cd_2Nb_2O_7$ [7] and by thermally induced reorientation of polarization of domains [18]. Next, relaxation caused by thermal displacements of the 'seventh' oxygen ions relative to Cd^{2+} ions is expected to contribute [19, 20]. Yet, no obvious evidence for the contribution of pressure-independent relaxation has been presented earlier. The purpose of this paper is to elucidate the nature of low-frequency dielectric relaxation in $Cd_2Nb_2O_7$ ferroelectric–ferroelastics over the temperature range from 100 to 300 K. For this reason, the complex dielectric permittivity of $Cd_2Nb_2O_7$ single crystals over the frequency range 1 kHz–1 MHz was studied in a wide measurement AC field strength range 1 V cm^{-1} $< \mathcal{E} <$ 110 V cm^{-1} including both weak and strong fields. To reduce domain relaxation, measurements were made on single crystals under a uniaxial pressure of 0 MPa $\leqslant X \lesssim 4$ MPa. The Curie–Weiss constant C_{CW}, temperature T_{max} and Arrhenius plots were derived from these data and their frequency-, $\mathcal{E}$- and pressure-induced changes were examined.

2. Experiment

$Cd_2Nb_2O_7$ single crystals were grown by the flux method [3]. The crystals from different batches had different colours; this is due to their non-ideal stoichiometry [2, 3, 13]. With this in mind, one can understand the absence of agreement in the phase transition temperatures of $Cd_2Nb_2O_7$ cited in the literature [7, 13, 14, 21]. The x-ray diffraction data at room temperature confirm the pyrochlore structure of crystals of different colours (colourless, yellow and orange) [2, 3, 5, 6]. Here, the dielectric relaxation was studied on colourless and light-yellow crystals for which the departure from ideal $Cd_2Nb_2O_7$ stoichiometry was the least [3, 5]. EDXA studies of stoichiometry of single crystals of different colours as well as dielectric studies of these crystals will be published elsewhere.

As-grown $[111]_{cub}$ platelets and $[100]_{cub}$ platelets cut perpendicular to the $[100]_{cub}$ axis ($P_s \| [100]_{cub}$ [3, 7]) were measured. Gold electrodes were evaporated onto the polished $(111)_{cub}$ and $(100)_{cub}$ surfaces. The platelet was placed between two plane-parallel Ag punches used as electrodes at the same time. One punch was firmly fixed in the cryostat while the other was movable. A uniaxial pressure was applied to the movable punch through a hinge–spring system. To avoid non-uniformity of the electric field and of the mechanical stress, the area of the movable punch was chosen to cover the whole surface of the platelet (10–12 mm^2 in area). The platelet under pressure was cooled to 80 K. At a fixed frequency, the complex dielectric permittivity $\varepsilon^* = \varepsilon' - i\varepsilon''$ (capacitance and losses) was measured on heating from 80 to 300 K at a rate of 2.5 K min^{-1}. Conventional capacitance bridges hp 4270 A (1 kHz–1 MHz) and TESLA BM-484 (1.592 kHz) were used. The temperature was stabilized to ± 0.5 K during the entire experiment.

3. Results

$\varepsilon'(T)$, $\varepsilon''(T)$ and $\tan\delta$ for frequencies of 1 kHz–1 MHz and various AC field strengths and pressures are presented in figures 1–5. The dielectric permittivity and $\tan\delta$ for $X = 1.5$ MPa were chosen because they change considerably when the pressure is increased to 1.5–2 MPa. When the pressure is over 2 MPa, their further change is insignificant. The observed behaviour of the permittivity and losses is assigned to a pressure-induced change in domain structure, as observed in [6, 18]. Nevertheless, the dielectric permittivity and losses are apparently influenced by the AC field strength and frequency. The frequency-, field $\mathcal{E}$- and pressure-induced changes in $\varepsilon'(T)$, $\varepsilon''(T)$ and $\tan\delta$ are found to be similar for the $[111]_{cub}$, $[100]_{cub}$ and $[110]_{cub}$ platelets (see also [6, 14]). An analysis of experimental data shows that, in addition to domain relaxation, one has to take into account relaxation which is independent of the uniaxial pressure of 0 MPa $< X <$ 4 MPa while it is frequency and $\mathcal{E}$ dependent.

3.1. $\varepsilon'(T)$, $\varepsilon''(T)$ and $\tan\delta$ for $X = 0$ MPa

Between 100 and 196 K (ferroelectric phase) the dielectric permittivity and losses become highly dispersive (figures 1(*a*), 2(*a*) and 3(*a*)). The character of the dielectric dispersion implies the existence of several mechanisms responsible for the dielectric relaxation phenomena. Indeed, when the frequency is reduced, the peak in $\varepsilon'(T)$ at T_{max} increases and shifts to a lower temperature. The peak in $\varepsilon''(T)$ and the peak in $\tan\delta$ shift to a lower temperature also and broaden. The difference in temperature for the peaks in $\varepsilon'(T)$ and $\varepsilon''(T)$ increases as the frequency decreases. Below 10 kHz, the ε'' versus T and the $\tan\delta$ versus T curves are asymmetric on the high-temperature side of the peak. Above 100 kHz, the curves become asymmetric on the low-temperature side. The asymmetric part of the curves covers the temperature interval 130–180 K. Both the magnitudes and the positions of the peaks in $\varepsilon'(T)$, $\varepsilon''(T)$ and $\tan\delta$ are strongly dependent on the AC field strength as well. The observed complex behaviour of the dielectric permittivity and losses for $X = 0$ MPa cannot be explained unambiguously except that the dominant dielectric relaxation is probably caused by the ferroelectric domain effect, in agreement with the conclusions in [7, 12–18]. Figures 4 and 5 show $\varepsilon'(T)$ and $\tan\delta$ along the $[100]_{cub}$ axis where the relaxation caused by ferroelectric domains is expected to be stronger.

3.2. $\varepsilon'(T)$, $\varepsilon''(T)$ and $\tan\delta$ for $X \neq 0$ MPa

The pressure-induced changes in dielectric permittivity and losses are as follows (figures 1–3). The values of the dielectric permittivity and $\tan\delta$ decrease noticeably. The peaks in $\varepsilon'(T)$, $\varepsilon''(T)$ and $\tan\delta$ shift to a higher temperature on approaching T_c. The ferroelectric transition temperature T_c and the ferroelastic transition temperature T_s increase. The former temperature changes at a rate of $dT_c/dX \simeq 4.3$ K MPa^{-1}, which is typical of other ferroelastics. This rate was estimated in [6] from the pressure-induced shift in P_s versus T and the pyroelectric current versus T curves within 100–300 K. The latter transition temperature changes at a rate of $dT_s/dX \simeq 0.046$ K MPa^{-1}, which is two orders of magnitude lower. This rate was estimated from the pressure-induced shift in the ε' versus T curve in the temperature range 180–300 K in [22] and causes some confusion. Indeed, if dT_s/dX were so low, at $X \simeq 2.2$ MPa the temperatures T_c and T_s would coincide and a further shift in the peaks in $\varepsilon'(T)$, $\varepsilon''(T)$ and $\tan\delta$ would immediately slow down; this is not observed (figures 1–3; see also figures 7 and 8 later and [6, 18, 22]). The ε'' versus T curve and $\tan\delta$ versus T curve become more symmetric whereas a well pronounced 'shoulder'

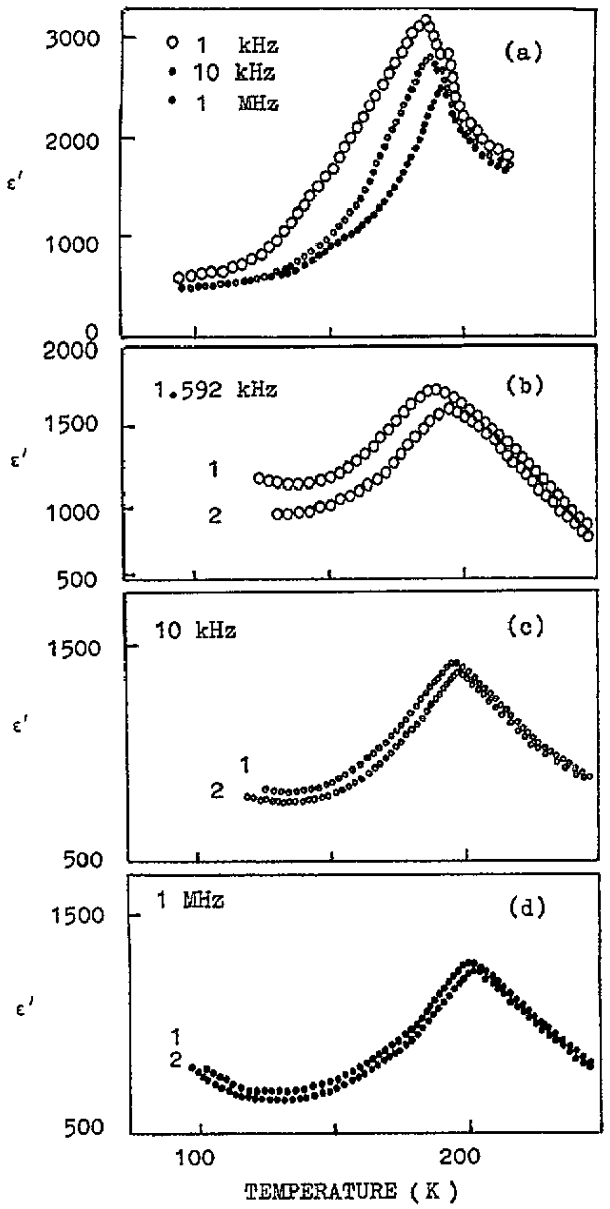

Figure 1. ε' versus T in the $[111]_{cub}$ platelet for various frequencies, AC field strengths and pressures. (*a*) $X = 0$ MPa: ○, 1 kHz, 1 V cm^{-1}; ○, 2 V cm^{-1}; ●, 1 MHz, 2 V cm^{-1}. (*b*) $X = 1.5$ MPa: (curve 1, 1.592 kHz, 100 V cm^{-1}; curve 2, 1 kHz, 25 V cm^{-1}. (*c*) $X = 1.5$ MPa: curve 1, 10 kHz, 12.5 V cm^{-1}; curve 2, 10 kHz, 2.5 V cm^{-1}. (*d*) $X = 1.5$ MPa: curve 1, 1 MHz, 12.5 V cm^{-1}; curve 2, 1 MHz, 2.5 V cm^{-1}.

appears on the low-temperature side of the peak (temperature interval 130–170 K). It is worth noting that dielectric dispersion still takes place both in the ferroelectric phase and in the paraelectric phase. The changes in $\varepsilon'(T)$, $\varepsilon''(T)$ and $\tan\delta$ caused by uniaxial pressure are the same for a strong AC field $\mathcal{E}$ of 100 V cm^{-1} when reorientation of domain polarization is dominant as for a weak AC field $\mathcal{E}$ of 2 V cm^{-1} when domain wall motion is dominant. The

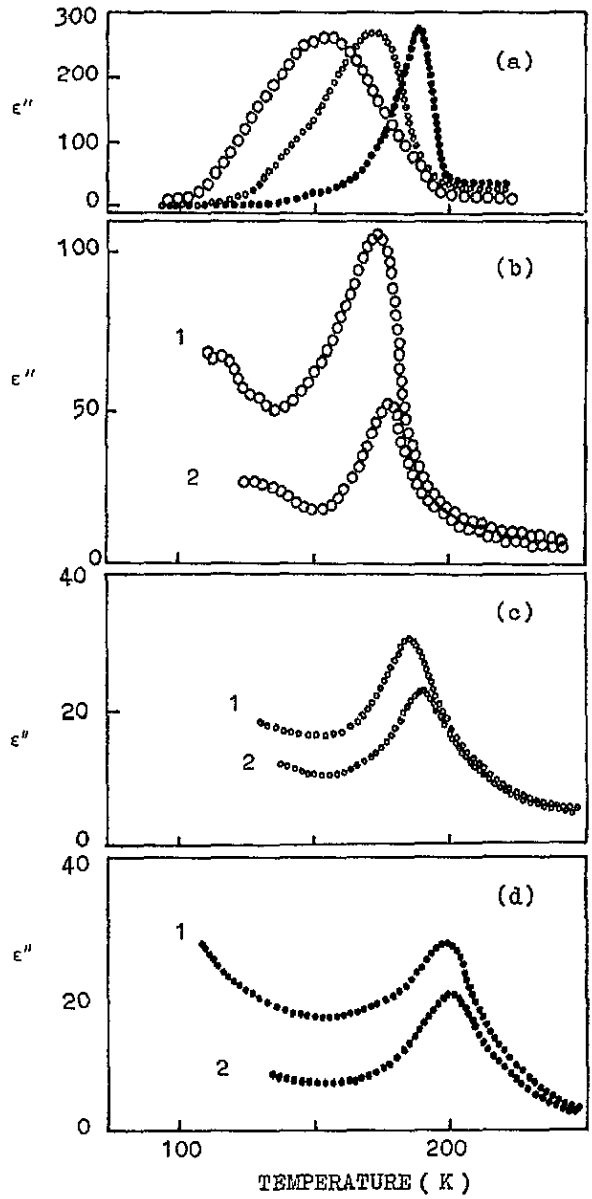

Figure 2. ε'' versus T in the $[111]_{cub}$ platelet for various frequencies, AC field strengths and pressures. The notation is the same as for figure 1.

existence of pressure-dependent domain relaxation is strongly supported by these data. On the other hand, for a pressure up to 4 MPa the frequency and $\mathcal{E}$ dependences of permittivity and losses in the ferroelectric phase remain persistent and significant (figures 1–3). This implies that domain effects alone cannot be responsible for their complex behaviour. When the AC field strength is increased or the frequency is decreased, $\varepsilon'(T), \varepsilon''(T)$ and $\tan\delta$ increase in magnitude, their peaks shift to a lower temperature and the 'shoulder' increases. That the AC field gives rise to a considerably higher 'shoulder' may also be associated with

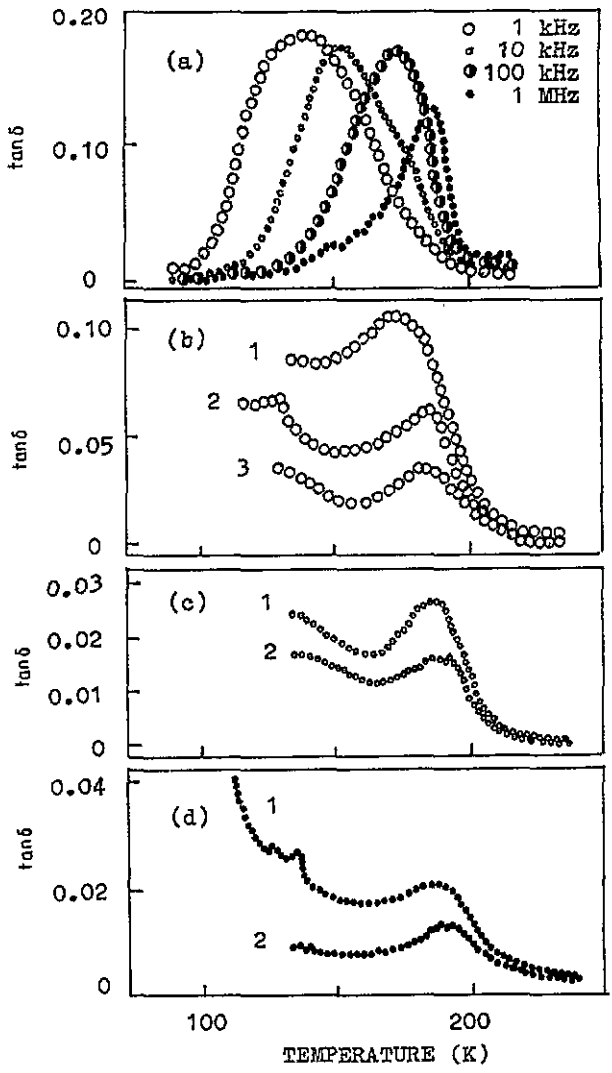

Figure 3. $\tan\delta$ versus T in the $[111]_{cub}$ platelet for various frequencies, AC field strengths and pressures. The notation is the same as for figure 1 except for (*b*): curve 1, 1.592 kHz, 100 V cm^{-1}; curve 2, 1.592 kHz, 80 V cm^{-1}; curve 3, 1 kHz, 25 V cm^{-1}.

the fact that the ion movement effect [23] plays an important role in the ferroelectric phase.

3.3. Curie–Weiss constant versus X

The Curie–Weiss constant was derived from the temperature dependences of the reciprocal dielectric constant in a conventional way [23]. These dependences for $Cd_2Nb_2O_7$ are available for $X = 0$ MPa, 4 V cm^{-1} $< \mathcal{E} <$ 50 V cm^{-1}, 100 Hz $< f <$ 1 MHz [3, 12, 14, 17] and for X equal to 2 and 4 MPa, $\mathcal{E}$ equal to 18 and 26 V cm^{-1}, 1 kHz $< f <$ 1 MHz [6]. For 205–260 K, the Curie–Weiss law applies to these dependences, i.e. $(\varepsilon')^{-1}_{T>T_c} = (T - T_0)/C_{CW}$, where T_0 is the Curie–Weiss temperature. Here, an analysis of the $(\varepsilon')^{-1}$ versus T dependences for pressure from 0 to 4 MPa, $\mathcal{E}$ from 1 to 110 V cm^{-1} and frequencies from

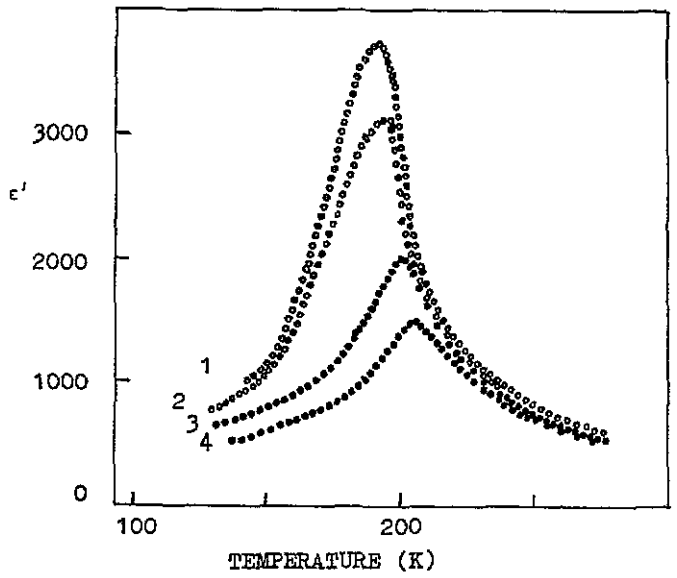

Figure 4. ε' versus T in the $[100]_{cub}$ platelet for $X = 0$ MPa and various frequencies and $\mathcal{E}$: curve 1, 10 kHz, 12.5 V cm^{-1}; curve 2, 10 kHz, 2.5 V cm^{-1}; curve 3, 1 MHz, 12.5 V cm^{-1}; curve 4, 1 MHz, 2.5 V cm^{-1}.

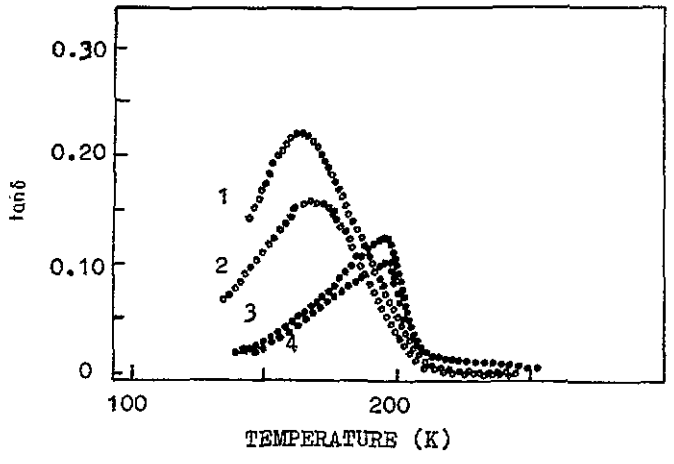

Figure 5. $\tan\delta$ versus T in the $[100]_{cub}$ platelet for $X = 0$ MPa and various frequencies and $\mathcal{E}$. The notation is the same as for figure 4.

1 kHz to 1 MHz also confirms their Curie–Weiss behaviour. This is why the corresponding plots are not presented in this paper. The Curie–Weiss constant versus pressure dependences for various frequencies and AC field strengths obtained from these plots are shown in figure 6. The frequency and $\mathcal{E}$ are chosen to work in only one way, i.e. to increase $\varepsilon'(T)$ and hence C_{CW}. The main change in C_{CW} results from uniaxial pressure, as is shown for 1 MHz and $\mathcal{E} = 2$ V cm^{-1} *when the dielectric relaxation originates from domains* [6, 12, 15, 17]. The Curie–Weiss constant displays a rapid drop from 1.2×10^5 to 0.6×10^5 K with increasing pressure. However, for pressures over 1.5 MPa it decreases more slowly. Over the whole

range of pressures used, the Curie–Weiss constant remains apparently frequency and $\mathcal{E}$ dependent. When the AC field strength is increased and/or the frequency is decreased, C_{CW} decreases more slowly (curves 1 and 2). The curves for frequencies over the range 1 MHz–1 kHz and for $\mathcal{E}$ up to 110 V cm^{-1} exhibit a tendency to converge at pressures higher than 3 MPa, gradually approaching curve 3. The C_{CW}-value of about 10^5 K for $X \neq 0$ MPa remains characteristic of the displacive-type phase transition [3, 12].

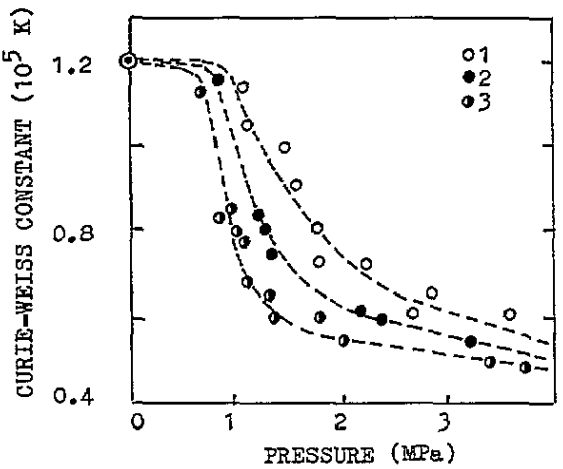

Figure 6. C_{CW} versus X along the $[111]_{cub}$ axis for various frequencies and $\mathcal{E}$ working to increase C_{CW}: curve 1, 1.592 kHz, 106 V cm^{-1}; curve 2, 10 kHz, 12.5 V cm^{-1}; curve 3, 1 MHz; 2 V cm^{-1}.

3.4. T_{max} versus X

To clarify the role of domains in the appearance of the peak in $\varepsilon'(T)$ at T_{max}, the pressure dependences of T_{max} for various $\mathcal{E}$ and frequencies have been compared. The temperature T_{max} exhibits an upward shift as the pressure is increased, with T_{max} for 1 and 10 kHz approaching $T_{max} \equiv T_c$ for 1 MHz in a weak AC field (figure 7). On the other hand, T_{max} shifts downwards with increeasing AC field strength. The lower the frequency, the more marked is the shift (figure 8). As a result, T_{max} for 1 and 10 kHz approaches $T_{max} \equiv T_c$ at a higher pressure. For an AC field $\mathcal{E} \gtrsim 80$ V cm^{-1}, these temperatures could converge at a pressure ($X \gg 4$ MPa) considerably higher than the conventional pressure which changes the domain structure [6] and $\varepsilon'(T)$, $\varepsilon''(T)$ and $\tan\delta$ (figures 1–3). This means that the $\mathcal{E}$- and frequency-stimulated change in the position of the peak in $\varepsilon'(T)$ can no longer be ascribed to domains only. There is another mechanism which can be responsible for the observed change in $\varepsilon'(T)$ at T_{max}. With increasing $\mathcal{E}$ and/or decreasing frequency, this mechanism becomes more obvious; yet with changing pressure it does not manifest itself.

3.5. Arrhenius plots for various AC field strengths and X

The dielectric loss data were analysed by the Arrhenius formalism assuming the Debye-type relaxation [23]

$$f = f_0 \exp(-Q/kT)$$

where Q is the activation energy, $f_0 = 1/2\pi\tau_0$ is the pre-exponential factor related to the nature of the relaxation, k is the Boltzmann constant and T is the absolute temperature. Using the relation $\omega\tau = 1$ for a maximum in $\varepsilon''(T)$, the corresponding Arrhenius diagrams for various AC field strengths and pressures have been plotted (figure 9). In the figure the diagram for $X = 0$ MPa in a weak AC field of 1 V cm^{-1} (line 2) is also given. The experimental data for both $X = 0$ MPa and $X \neq 0$ MPa over a frequency range 1 kHz–1 MHz conform to two straight lines, which correspond to the existence of two relaxation processes (see also [12, 17] for data at $X = 0$ MPa). What is most striking is that both relaxation processes are affected by $\mathcal{E}$ and yet only the high-frequency relaxation process is affected by the pressure.

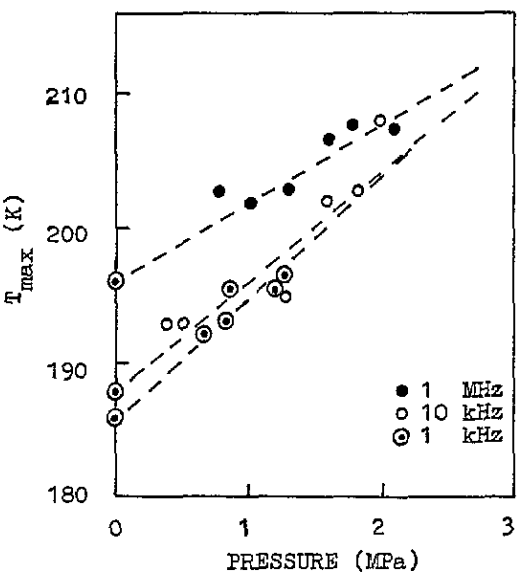

Figure 7. T_{max} versus X along the $[111]_{cub}$ axis for 1 kHz, 10 kHz and 1 MHz and a weak AC field $\mathcal{E}$ of 2.5 V cm^{-1}.

For $X = 0$ MPa, the relaxation which occurs at frequencies higher than 10 kHz is characterized by the activation energy $Q = 0.26$ eV and $\tau_0 \simeq 2.4 \times 10^{-13}$ s which are typical of the domain wall motion effect [23] ($Q = 0.17$ eV and $\tau_0 = 2.7 \times 10^{-14}$ s for $Cd_2Nb_2O_7$ ceramics [17]). As the AC field strength is increased, the straight lines shift to a lower temperature (line 1). As the pressure is increased, the straight lines shift to a higher temperature (lines 3–5). When X is greater than 2 MPa, the lines seem to shift insignificantly. At $X = 1.5$ MPa, $Q = 0.73$ eV, $\tau_0 \simeq 10^{-23}$–10^{-24} s for $\mathcal{E} = 2.5$ V cm^{-1} and $Q = 0.64$ eV, $\tau_0 \simeq 10^{-22}$ s for $\mathcal{E} = 12.5$ V cm^{-1}. As the dielectric relaxation rate becomes too small, a more general analysis of dielectric relaxation phenomena by the Cole–Cole formalism would be preferable. For the analysis, the dielectric studies over a wider frequency range involving lower frequencies would be needed.

The relaxation which occurs below 10 kHz is characterized by $Q = 0.16$–0.18 eV, $\tau_0 \simeq 10^{-9}$–10^{-11} s for $X = 0$ MPa and by $Q = 0.22$ eV, $\tau_0 \simeq 10^{-10}$–10^{-12} s for $X = 1.5$ MPa. In this case, the order of magnitude of the relaxation rate is typical of the ion and dipole movement effect [24, 25].

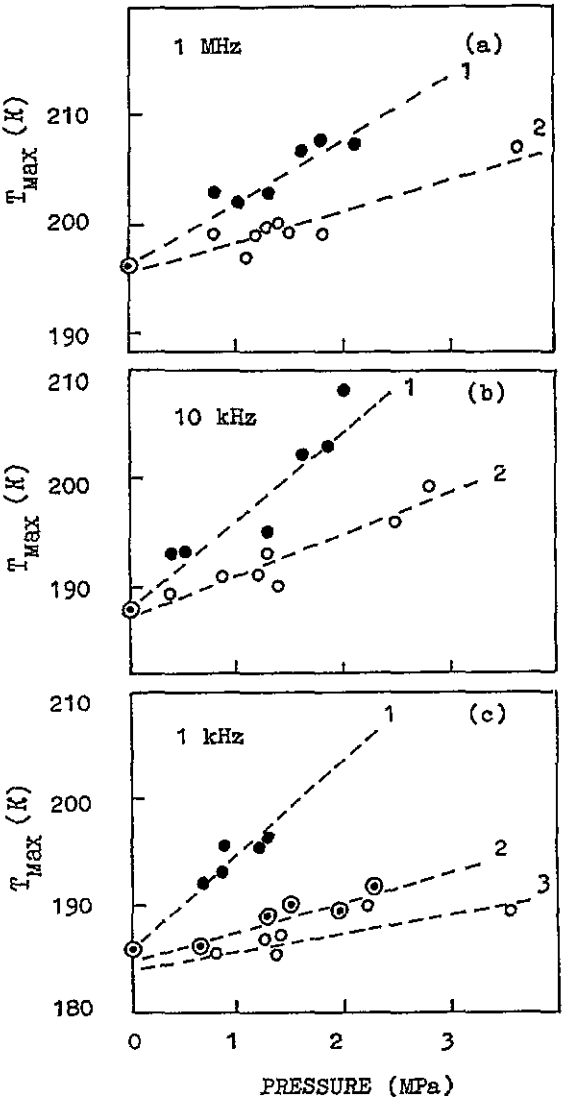

Figure 8. T_{max} versus X for various AC field strengths over the frequency range 1 kHz–1 MHz: (*a*) curve 1, 1 MHz, 2.5 V cm^{-1}; line 2, 1 MHz, 12.5 V cm^{-1}. (*b*) line 1, 10 kHz, 2.5 V cm^{-1}; line 2, 10 kHz, 12.5 V cm^{-1}. (*c*) line 1, 1 kHz, 2.5 V cm^{-1}; line 2, 1.592 kHz, 80 V cm^{-1}; line 3, 1.592 kHz, 106 V cm^{-1}.

4. Discussion

The pyrochlore structure can be described as a network structure of $(BO_6)^{n-}$ octahedra linked corner to corner, with the A cations and two Z anions filling the interstices (see [3] and references therein). The A cations are coordinated by eight anions within the $(AO_8)^{n-}$ polyhedra. Six equally spaced oxygen ions belong to both $(BO_6)^{n-}$ and $(AO_8)^{n-}$ polyhedra while two axial Z anions are located at a shorter distance from the central cation and are bonded to this cation only. That is why in the two-interpenetrating-networks description of the pyrochlore structure [26] the larger bond lengths in the $(AO_8)^{n-}$ polyhedra may be

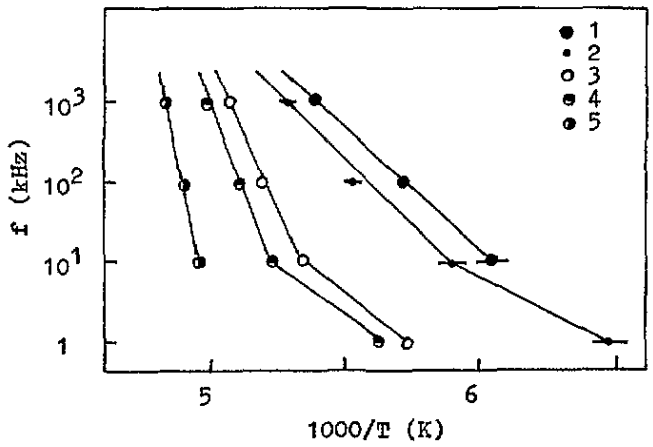

Figure 9. Arrhenius plots for various $\mathcal{E}$ and pressures: line 1, $X = 0$ MPa, 12.5 V cm^{-1}; line 2, $X = 0$ MPa, 1 V cm^{-1}; line 3, $X = 1.5$ MPa, 12.5 V cm^{-1}; line 4, $X = 1.5$ MPa, 2.5 V cm^{-1}; line 5, $X = 2.2$ MPa, 2.5 V cm^{-1}.

ignored and a linear coordination with the two closest Z anions may be assumed (identical with the Cu_2O network). This viewpoint is especially appropriate for the $Cd_2Nb_2O_7$ pyrochlore which has the most 'spacious' lattice of the oxide pyrochlores of $A_2^{2+}B_2^{5+}O_7$ type [3, 19, 20].

As the Cd^{2+} ions and especially the 'seventh' oxygen ions are weakly bonded to the $(NbO_6)^{n-}$ octahedra-forming network, the steady Cd^{2+}–O^{2-} (seventh) dipoles are rather mobile. Relative displacements of the ions in the external AC field would induce ionic polarizability as well as orientational polarizability of the steady dipoles. The competition between the orientational polarizability and thermally induced disorder of dipoles leads to domination of the former with decreasing temperature. In the ferroelectric phase, this mechanism, together with the ferroelectric and ferroelastic domains, is responsible for the observed dielectric relaxation phenomena in the frequency range 1 kHz–1 MHz. Keeping in mind that the system of disordered Cd–O dipoles is formed in the paraelectric phase, one may expect that their orientational polarizability in the AC field may cause an anomalously high $\varepsilon_0 = 450$ *compared with* $\varepsilon_\infty = 5.43$ *at room temperature as well as dielectric dispersion in* the paraelectric phase. It is a well known fact that this relaxation mechanism is responsible for the anomalously high $\varepsilon_0 = 81$ compared with $\varepsilon_\infty = 1.77$ for water [24] as well as for polar liquids. According to the Debye model [24], the relaxation time $\tau = 4\pi\eta a^3/kT$ and orientational polarizability of molecules $\alpha = \alpha_0/(1 + i\omega\tau)$ depend on the viscosity η. On the assumption that the molecule radius $a \simeq 10^{-8}$ cm and $\tau \simeq 10^{-4}$–10^{-5} s (see figure 9), the viscosity η for the $(CdO_8)^{n-}$ polyhedra-forming network in $Cd_2Nb_2O_7$ at 150 K is about 10^4–10^5 P. This value is well within the range of η for viscous liquids and vitreous oxides above the softening point [25, 27].

5. Conclusions

Dielectric studies of $Cd_2Nb_2O_7$ single crystals under a uniaxial pressure of 0 MPa $\leqslant X \lesssim$ 4 MPa over a wide measurement AC field strength range 1–110 V cm^{-1} give new insight into the nature of the dielectric relaxation phenomena within the frequency range 1 kHz–1 MHz.

In the ferroelectric phase, two relaxation mechanisms are responsible for the frequency-, $\mathcal{E}$- and pressure-induced changes in $\varepsilon'(T)$, $\varepsilon''(T)$ and $\tan\delta$. In addition to the dominant relaxation caused by ferroelastic and ferroelectric domains, there is also relaxation caused by the orientational polarizability of the steady Cd^{2+}–O^{2-} (seventh) dipoles in the external AC field. The system of disordered dipoles in the pyrochlore network is formed in the paraelectric phase and is supposed to be a precursor of the glassy state in $Cd_2Nb_2O_7$ below 18 K [11]. As far as we know, the cubic oxide pyrochlore $Cd_2Nb_2O_7$ is the first example of a ferroelectric in which ferroelectric and ferroelastic domains and a disordered dipole system exist simultaneously [1].

Acknowledgments

The authors are grateful to Professor B Hilczer for the support given by the research programme. We also thank Dr E S Sher for providing the $Cd_2Nb_2O_7$ single crystals used in this work.

References

[1] *Landolt–Börnstein New Series* 1981 Group III, vol 16a (Berlin: Springer)
[2] Brisse F, Stewart D J, Seidl V and Knop O 1972 *Can. J. Chem.* **50** 3648
[3] Jona F, Shirane G and Pepinsky R 1955 *Phys. Rev.* **98** 903
[4] *International Tables for X-ray Crystallography* 1965 vol 1 (Birmingham: Kynoch)
[5] Kolpakova N N, Pietraszko A, Waplak S and Szczepanska L 1991 *Solid State Commun.* **79** 707
[6] Kolpakova N N, Margraf R and Pietraszko A 1987 *Fiz. Tverd. Tela* **29** 2638
[7] Ye Z G, Kolpakova N N, Rivera J-P and Schmid H 1991 *Ferroelectrics* **124** 275
[8] Shirane G and Pepinsky R 1953 *Phys. Rev.* **92** 504
[9] Smolensky G A, Kolpakova N N, Kizhaev S A and Sher E S 1987 *Ferroelectrics* **73** 161
[10] Lawless W N, Anderson A C and Walker F 1981 *Ferroelectrics* **37** 627
[11] Kolpakova N N, Hilczer B and Wiesner M 1993 *Phase Trans.* at press
[12] Kolpakova N N, Siny I G, Polomska M and Margraf R 1982 *Fiz. Tverd. Tela* **24** 1729
[13] Markovin P A, Pisarev R V, Sher E S and Shermatov B N 1983 *Fiz. Tverd. Tela* **25** 3642
[14] Isupov V A and Tarasova G I 1983 *Fiz. Tverd. Tela* **25** 1018
[15] Banys J, Grigas J, Kolpakova N N, Sobestijanskas R and Sher E 1989 *Lithuanian J. Phys.* **29** 209
[16] Smolensky G A, Kolpakova N N, Kizhaev S A *et al* 1984 *Fiz. Tverd. Tela* **26** 989
[17] Swartz S L, Randall C A and Bhalla A S 1989 *J. Am. Ceram. Soc.* **72** 637
[18] Kolpakova N N, Sher E S and Waplak S 1990 *Ferroelectrics* **111** 257
[19] Kolpakova N N, Polomska M and Margraf R 1990 *Fiz. Tverd. Tela* **32** 1893
[20] Kolpakova N N, Polomska M and Wolak J 1992 *Ferroelectrics* **126** 151
[21] Smolensky G A, Krainik N N, Kamzina L S *et al* 1985 *Japan. J. Appl. Phys.* **24** (Supplement 24-2 820)
[22] Salaev F M, Kamzina L S and Krainik N N 1992 *Fiz. Tverd. Tela* **34** 1843
[23] Burfoot J C 1979 *Polar Dielectrics and Their Applications* (London: Macmillan)
[24] Kittel Ch 1956 *Introduction to Solid State Physics* (New York: Wiley)
[25] Stevels J M 1962 *Encyclopedia of Physics* vol XIII *Thermodynamics of Liquids and Solids* ed S Flügge (Berlin: Springer) pp 510–645
[26] McCauley R A 1980 *J. Appl. Phys.* **51** 290
[27] Ebert H 1957 *Physikalisches Taschenbuch* (Braunschweig: Vieweg)